

# Training and validation of a deep learning architecture for the automatic analysis of coronary angiography

Tianming Du<sup>1</sup>, PhD; Lihua Xie<sup>2</sup>, MSc; Honggang Zhang<sup>1</sup>, PhD; Xuqing Liu<sup>1</sup>, PhD; Xiaofei Wang<sup>3</sup>, MSE; Donghao Chen<sup>3</sup>, MSE; Yang Xu<sup>3</sup>, BSE; Zhongwei Sun<sup>2</sup>, MSc; Wenhui Zhou<sup>3</sup>, PhD; Lei Song<sup>2</sup>, MD; Changdong Guan<sup>2</sup>, MSc; Alexandra J. Lansky<sup>4</sup>, MD; Bo Xu<sup>2\*</sup>, MBBS

1. Beijing University of Posts and Telecommunications, Beijing, China; 2. Fu Wai Hospital, National Center for Cardiovascular Diseases, Chinese Academy of Medical Sciences, Beijing, China; 3. Beijing Redcdn Technology Co., Ltd, Beijing, China; 4. Yale University School of Medicine, New Haven, CT, USA

T. Du and L. Xie contributed equally to this work.

This paper also includes supplementary data published online at: <https://eurointervention.pconline.com/doi/10.4244/EIJ-D-20-00570>

## KEYWORDS

- artificial intelligence
- coronary artery disease
- imaging modalities
- multiple vessel disease

## Abstract

**Background:** In recent years, the use of deep learning has become more commonplace in the biomedical field and its development will greatly assist clinical and imaging data interpretation. Most existing machine learning methods for coronary angiography analysis are limited to a single aspect.

**Aims:** We aimed to achieve an automatic and multimodal analysis to recognise and quantify coronary angiography, integrating multiple aspects, including the identification of coronary artery segments and the recognition of lesion morphology.

**Methods:** A data set of 20,612 angiograms was retrospectively collected, among which 13,373 angiograms were labelled with coronary artery segments, and 7,239 were labelled with special lesion morphology. Trained and optimised by these labelled data, one network recognised 20 different segments of coronary arteries, while the other detected lesion morphology, including measures of lesion diameter stenosis as well as calcification, thrombosis, total occlusion, and dissection detections in an input angiogram.

**Results:** For segment prediction, the recognition accuracy was 98.4%, and the recognition sensitivity was 85.2%. For detecting lesion morphologies including stenotic lesion, total occlusion, calcification, thrombosis, and dissection, the F1 scores were 0.829, 0.810, 0.802, 0.823, and 0.854, respectively. Only two seconds were needed for the automatic recognition.

**Conclusions:** Our deep learning architecture automatically provides a coronary diagnostic map by integrating multiple aspects. This helps cardiologists to flag and diagnose lesion severity and morphology during the intervention.

\*Corresponding author: Fu Wai Hospital, National Center for Cardiovascular Diseases, Chinese Academy of Medical Sciences, A 167, Beilishi Road, Xicheng District, Beijing, 100037, China. E-mail: [bxu@citmd.com](mailto:bxu@citmd.com)

## Abbreviations

<b>AI</b>	artificial intelligence
<b>CVD</b>	cardiovascular diseases
<b>DNN</b>	deep neural networks
<b>LAD</b>	left anterior descending
<b>LCX</b>	left circumflex artery
<b>LM</b>	left main
<b>OM</b>	obtuse marginal
<b>RCA</b>	right coronary artery
<b>TO</b>	total occlusion

## Introduction

Coronary artery disease (CAD) is the most common cardiovascular disease<sup>1</sup>, and the leading cause of death globally during the past two decades<sup>2</sup>. Therefore, the diagnosis and prevention of CAD is crucial for modern society. Coronary angiography (CAG), which provides assessments of luminal stenosis, plaque characteristics, and disease activity, is an important tool for CAD diagnosis and treatment guidance<sup>3,4</sup>. In recent years, the use of deep learning has become more commonplace in the biomedical field and its development will greatly assist clinical and imaging data interpretation<sup>5</sup>. Deep learning can simplify the procedure by directly learning predictive features, thereby strongly supporting the translation from artificial algorithms into clinical application<sup>6-8</sup>. However, much of the previous work to apply deep learning algorithms in the field of CAD has focused on single aspects of the analysis of the coronary artery, such as vessel segmentation<sup>9,10</sup>, coronary artery centreline extraction<sup>11</sup>, noise reduction<sup>12</sup>, coronary artery geometry synthesis<sup>13</sup>, coronary plaque characterisation<sup>14</sup>, and calcification detection. Thus, there remains a large gap between the results produced by the aforementioned algorithms and the actual diagnosis of CAD.

High diagnostic accuracy from a coronary angiogram requires correct recognition of lesion morphology and location. Herein, to tackle the above recognition tasks, two unique functional deep neural networks (DNN) were proposed, on which we created, trained, validated, and then tested a coronary angiography recognition system called DeepDiscern. DeepDiscern was evaluated on a test data set of consecutive angiograms collected from clinical cases.

Editorial, see page 16

## Methods

### STUDY POPULATION AND IMAGE ACQUISITION

To develop the DeepDiscern system, 20,612 angiograms from 10,073 patients were consecutively collected using the image acquisition data from a large single centre (Fu Wai Hospital, National Center for Cardiovascular Diseases, Beijing, China). For coronary segmentation DNN training, 13,373 angiograms were consecutively collected from 2,834 patients who underwent CAGs in July 2018. The remaining 7,239 angiograms, with at least one identifiable lesion morphology, such as stenotic lesion, total occlusion (TO), calcification, thrombus, and dissection, collected from 7,239 patients, were used for lesion morphology recognition. The collected angiogram information is listed in **Table 1**.

**Table 1. Baseline patient and lesion characteristics.**

Coronary artery recognition	
Patients	(N=2,834)
Age, years	61.6±17.5
Female	29.9% (848)
Left dominance	24.1% (683)
Segmentation	(N=13,373)*
LM	77.7% (10,390)
LAD	64.2% (8,594)
DIA	51.3% (6,854)
LCX	36.6% (4,890)
OM	36.6% (4,890)
L-PLA	36.6% (4,890)
L-PDA	36.6% (4,890)
RCA	22.3% (2,983)
PDA	22.3% (2,983)
PLA	22.3% (2,983)
Lesion morphology detection	
Patients	(N=7,239)
Age, years	65.5±16.0
Female	20.9% (1,513)
Left dominance	22.8% (1,650)
Lesion morphology	(N=12,184)†
Stenosis (DS ≥50%)	22.2% (2,700)
Total occlusion	36.6% (4,458)
Lesion bending >45°	44.2% (1,970)
Lesion length	17.6±13.2
≥20 mm	24.2% (1,079)
Blunt stump	37.2% (1,658)
Moderate or heavy calcification	19.5% (2,378)
Thrombus	11.8% (1,439)
Dissection	10.0% (1,209)

\* The number of angiograms in the coronary artery recognition task. † The number of lesion samples in the lesion morphology detection task. DIA: diagonal; LAD: left anterior descending artery; LCX: left circumflex artery; LM: left main; L-PDA: left posterior descending; L-PLA: left posterolateral; OM: obtuse marginal; PDA: posterior descending; PLA: posterolateral; RCA: right coronary artery

Raw angiographic data for our work were acquired during interventional procedures of patients and saved in 512×512-pixel digital imaging and communications in medicine (DICOM) format with angiographic views and video information, without patient identifiers. Each patient's angiographic DICOM included several angiographic sequences encompassing different angiographic views. The choice of angiographic views was left to the operator's discretion, to delineate best the lesion severity and morphology. In general, the angiographic views for the left coronary artery included CRA (cranial view), CAU (caudal view), LAO\_CRA (left anterior oblique-cranial view), LAO\_CAU (left anterior oblique-caudal view), RAO\_CRA (right anterior oblique-cranial view), and RAO\_CAU (right anterior oblique-caudal view). For the right coronary artery the views included LAO, LAO\_CAU, LAO\_CRA and RAO. The data flow is presented in **Figure 1**.

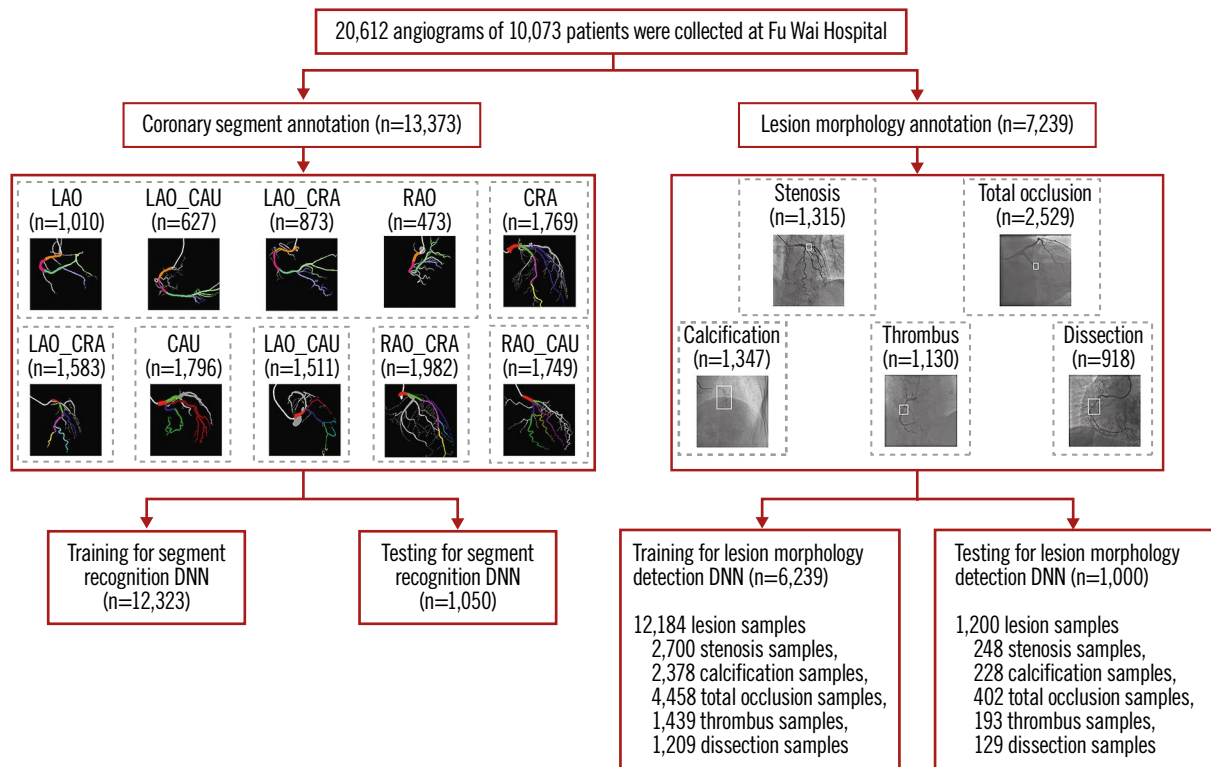


**Figure 1.** Data flow for the lesion morphology detection task and the coronary segment recognition task. *Coronary segment recognition.* In total, 13,373 angiograms were used, and divided into seven parts to train and test DeepDiscern DNN. *Lesion morphology detection.* In total, 7,239 angiograms with 1 to 3 lesion morphology were labelled for model training and testing. There were 12,184 lesion samples of five kinds of lesion morphology. CAU: caudal view; CRA: cranial view; LAO: left anterior oblique view; LAO\_CAU: left anterior oblique-caudal view; LAO\_CRA: left anterior oblique-cranial view; RAO: right anterior oblique view; RAO\_CAU: right anterior oblique-caudal view; RAO\_CRA: right anterior oblique-cranial view

## REFERENCE STANDARD AND ANNOTATION PROCEDURES

DeepDiscern learns rules from the labelled images in the training phase. To this end, all angiograms collected over a period of 11 months for the training and testing data sets were reviewed by ten qualified analysts in the angiographic core lab at Fu Wai Hospital. Coronary segments were annotated based on pre-established diagnostic criteria and lesion morphology characterised.

For the coronary segment recognition data sets, each angiogram was labelled at a pixel-by-pixel level for coronary segmentation recognition. First, analysts annotated sketch labels of all coronary artery segments on the original angiograms, with different colours representing different arterial segments. Then a group of trained and certified technicians labelled fine ground-truth images pixel by pixel according to the sketch labels. **Supplementary Figure 1** illustrates this process.

A total of 20 coronary artery segments were annotated (**Supplementary Figure 2**), including proximal right coronary artery (RCA prox), RCA mid, RCA distal, right posterior descending (PDA), right posterolateral, left main (LM), proximal left anterior descending (LAD prox), LAD mid, LAD distal, 1st diagonal, add. 1st diagonal, 2nd diagonal, add. 2nd diagonal, proximal circumflex (LCX prox), LCX distal, 1st obtuse marginal (OM), 2nd OM, left posterolateral, left posterior descending (L-PDA) and intermediate.

Although accurate coronary diagnosis requires coronary injections in multiple views to ensure that all coronary segments are seen clearly without foreshortening or overlap, it is not necessary to include all potential views in a given coronary segment. In clinical practice, several dominant projections are typically used to visualise a coronary segment and its morphology. Therefore, during the training and testing process of each coronary segment, DeepDiscern focused mainly on dominant projections provided. The corresponding relationship between the observed coronary segment and the angiographic views is shown in **Supplementary Table 1**.

For the lesion morphology detection data sets, expert analysts marked all lesion morphologies identified on the angiogram, including stenotic lesion, TO, calcification, thrombosis, and dissection. Stenotic lesion was defined as  $\geq 50\%$  diameter stenosis. TO was defined as angiographic evidence of TOs with Thrombolysis In Myocardial Infarction (TIMI) flow grade 0. Calcification was defined as readily apparent radiopacities noted within the apparent vascular wall (moderate: densities noted only with cardiac motion before contrast injection; severe: radiopacities noted without cardiac motion before contrast injection). Thrombus was defined as a discrete, intraluminal filling defect with defined borders and largely separated from the adjacent wall with or without contrast staining<sup>15</sup>. Dissection grade was diagnosed based on the National

Heart, Lung and Blood Institute (NHLBI) coronary dissection criteria (**Supplementary Table 2**). The lesion type, location, and extent were labelled using a rectangular box. **Supplementary Figure 1** illustrates this process. In total, 7,239 angiograms with one to three lesion morphologies were labelled for model training and testing. There were 12,184 positive samples in these angiograms. The lesion morphology classification data are shown in **Table 1**.

## DEEP LEARNING MODEL

DeepDiscern was designed to use these two DNN to recognise coronary segments and detect lesion morphology (**Figure 2**). Features of the input angiogram carrying different semantic information were extracted including low-level features, such as vessel edges and background texture, and high-level features, such as the overall shape of the arteries.

For the coronary artery recognition task, we modified a special DNN - conditional generative adversarial network (cGAN) (**Supplementary Figure 3**) for image segmentation. For the lesion morphology detection task, we developed a convolutional DNN (**Supplementary Figure 4**), which outputs the location of all the lesion morphologies that appeared in the input angiogram. The network structure, implementation details, training process and testing process of segment recognition DNN are detailed in **Supplementary Appendix 1**, and the lesion detection DNN in **Supplementary Appendix 2**.

For each input angiogram, DeepDiscern combines the two output results from coronary artery recognition DNN and lesion

morphology detection DNN to generate high-level diagnostic information, including identification of every coronary artery lesion and the coronary artery segment in which it is located.

## MODEL EVALUATION AND STATISTICAL ANALYSIS

For arterial segment recognition, given an input angiogram, the DeepDiscern segment recognition DNN produced an output image with several identified areas that represent the different coronary segments (**Supplementary Table 3**). For each coronary segment, we calculated the predicted pixel number for true positive (TP), true negative (TN), false positive (FP) and false negative (FN). Based on these results, we evaluated the segment recognition model by several metrics including accuracy ( $(TP+TN)/[TP+TN+FP+FN]$ ), sensitivity ( $TP/[TP+FN]$ ), specificity ( $TN/[TN+FP]$ ), positive predictive value ( $TP/[TP+FP]$ ), and negative predictive value ( $TN/[TN+FN]$ ). The recognition model was evaluated using 1,050 images including all the coronary segments.

In terms of lesion morphology detection, the DeepDiscern lesion detection DNN predicts several rectangular areas containing the lesions to describe their location and type. For the algorithmic analysis, lesion morphology is detected correctly if the overlap rate of a predicted rectangle and the ground-truth rectangle (labelled by cardiologists) exceeds a threshold  $\lambda_d=0.5$ . We measured the performance of the lesion detection model using precision rate P, recall rate R, and F1 score. The precision rate is defined as the percentage of correctly detected lesion cases from all lesion cases detected by the models. The recall rate is defined as the percentage

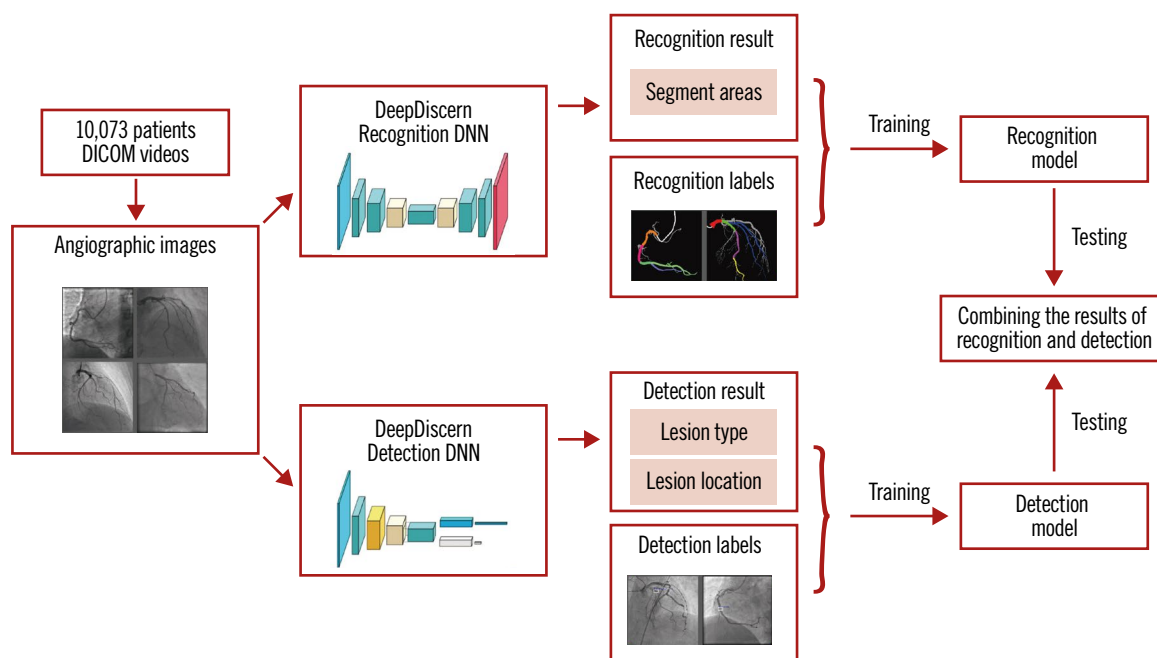


**Figure 2.** The workflow of DeepDiscern. In total, 20,612 angiographic images were collected from DICOM videos of 10,073 patients. Under the supervision of the labelled images, we trained the lesion morphology detection model and coronary artery recognition model of DeepDiscern. After training, the detection and recognition models generate the result images. These two results were combined to generate a high-level diagnosis.

of correctly detected lesions from all ground-truth lesions labelled by cardiologists. The F1 score [ $F_1 = 2 \times P \times R / (P + R)$ ], which combines the accuracy rate and recall rate, is a better measure of the overall performance of the detection DNN model. The evaluation process of the recognition model and of the detection model is illustrated in **Supplementary Figure 5**.

## Results

Coronary segment recognition DNN was evaluated using 1,050 images that included all the coronary segments. For segment prediction, the average accuracy, sensitivity, specificity, positive predictive value, and negative predictive value of all coronary artery segments was 98.4%, 85.2%, 99.1%, 76.2%, and 99.5%, respectively. Higher accuracy and sensitivity rates were observed in the proximal segments of major epicardial vessels (99.9% and 91.8% for LM, 99.8% and 92.6% for LAD proximal, 99.8% and 87.9% for LCX proximal, and 99.8% and 87.9% for RCA proximal). Arterial segments that were identified incorrectly were mostly in the distal segments and side branches of the major epicardial vessels. The performance of coronary segment recognition DNN was improved as the amount of data increased (**Supplementary Figure 6**). Because the majority of pixels in the image were negative, DNN performance cannot be assessed only from specificity and negative predictive value. **Table 2** provides detailed results including more metrics, and **Figure 3A** illustrates result images of the artery recognition task. The results under different angiographic views are shown in **Supplementary Table 4**.

One thousand angiograms were used to test the lesion morphology detection DNN model. The test data set included 1,200 (248 stenotic, 228 calcification, 402 TO, 193 thrombus, and 129 dissection) lesion samples. The F1 score, which represents the overall performance of the DNN model, for stenotic lesion, TO, calcification, thrombus, and dissection was 0.829, 0.810, 0.802, 0.823 and 0.854, respectively. For all lesion morphologies, recall rates were higher than precision rates. Results are shown in **Table 3** and examples of result images of the lesion morphology task are shown in **Figure 3B**. The receiver operating characteristic (ROC) curves for different lesion morphologies are shown in **Figure 4**. The area under the curve (AUC) of the lesion morphology detection

**Table 3. Diagnostic performance of DeepDiscern lesion detection DNN.**

Lesion type	Precision rate	Recall rate	F1 score
Stenosis	0.769	0.901	0.829
Total occlusion	0.757	0.871	0.810
Calcification	0.751	0.862	0.802
Thrombus	0.742	0.925	0.823
Dissection	0.790	0.926	0.854

DeepDiscern achieved an average recall of 89.7% for the five lesion types, namely, stenosis, total occlusion, calcification, thrombus and dissection ( $\lambda_d = 0.5$ ).

**Table 2. Performance of DeepDiscern segment recognition DNN for different coronary artery segments.**

Coronary artery segment	Accuracy % (95% CI)	Sensitivity % (95% CI)	Specificity % (95% CI)	PPV % (95% CI)	NPV % (95% CI)
All segments	98.4 (98.3-98.4)	85.2 (84.8-85.6)	99.1 (99.1-99.1)	76.2 (75.7-76.6)	99.5 (99.5-99.5)
LM	99.9 (99.9-99.9)	91.8 (91.1-92.5)	99.9 (99.9-99.9)	80.7 (79.4-82.0)	99.9 (99.9-99.9)
LAD proximal	99.8 (99.8-99.8)	92.6 (91.9-93.2)	99.9 (99.8-99.9)	80.9 (79.5-82.4)	99.9 (99.9-99.9)
LAD mid	99.8 (99.7-99.8)	90.8 (90.1-91.4)	99.8 (99.8-99.8)	82.1 (81.0-83.2)	99.9 (99.9-99.9)
LAD apical	99.7 (99.7-99.7)	84.5 (83.0-86.1)	99.8 (99.8-99.8)	67.8 (66.1-69.5)	99.9 (99.9-99.9)
1st DIA	99.4 (99.4-99.5)	78.1 (75.9-80.4)	99.6 (99.6-99.6)	60.0 (58.1-62.0)	99.8 (99.8-99.9)
2nd DIA	99.7 (99.7-99.8)	73.7 (68.0-79.3)	99.8 (99.8-99.8)	41.2 (36.5-45.9)	99.9 (99.9-99.9)
LCX proximal	99.8 (99.8-99.8)	87.9 (86.4-89.4)	99.9 (99.9-99.9)	78.8 (77.1-80.5)	99.9 (99.9-99.9)
LCX distal	99.7 (99.6-99.7)	81.3 (79.6-83.1)	99.8 (99.8-99.8)	78.3 (76.3-80.2)	99.9 (99.8-99.9)
Intermediate	99.6 (99.5-99.6)	74.1 (69.8-78.4)	99.7 (99.7-99.8)	63.2 (58.1-68.4)	99.9 (99.8-99.9)
OM	99.7 (99.6-99.7)	79.2 (75.9-82.5)	99.8 (99.7-99.8)	53.0 (48.8-57.2)	99.9 (99.9-99.9)
L-PLA	99.5 (99.5-99.5)	80.6 (78.3-82.8)	99.7 (99.6-99.7)	69.1 (66.7-71.4)	99.8 (99.8-99.9)
L-PDA	99.6 (99.5-99.7)	83.1 (79.6-86.6)	99.7 (99.7-99.8)	72.5 (69.1-75.9)	99.9 (99.9-99.9)
RCA proximal	99.8 (99.8-99.8)	87.9 (87.0-88.8)	99.9 (99.9-99.9)	86.7 (85.9-87.5)	99.9 (99.9-99.9)
RCA mid	99.7 (99.7-99.8)	85.6 (84.5-86.7)	99.8 (99.8-99.9)	76.6 (75.3-77.9)	99.9 (99.9-99.9)
RCA distal	99.8 (99.8-99.8)	83.2 (82.0-84.4)	99.9 (99.9-99.9)	88.2 (87.1-89.3)	99.9 (99.9-99.9)
PDA	99.7 (99.7-99.7)	75.4 (73.4-77.4)	99.8 (99.8-99.9)	70.6 (68.7-72.5)	99.9 (99.9-99.9)
PLA	99.5 (99.5-99.5)	77.2 (75.6-78.7)	99.7 (99.7-99.7)	72.0 (70.3-73.7)	99.8 (99.8-99.8)

CI: confidence interval; DIA: diagonal; LAD: left anterior descending artery; LCX: left circumflex artery; LM: left main; L-PDA: left posterior descending; L-PLA: left posterolateral; NPV: negative predictive value; OM: obtuse marginal; PDA: posterior descending; PLA: posterolateral; PPV: positive predictive value; RCA: right coronary artery

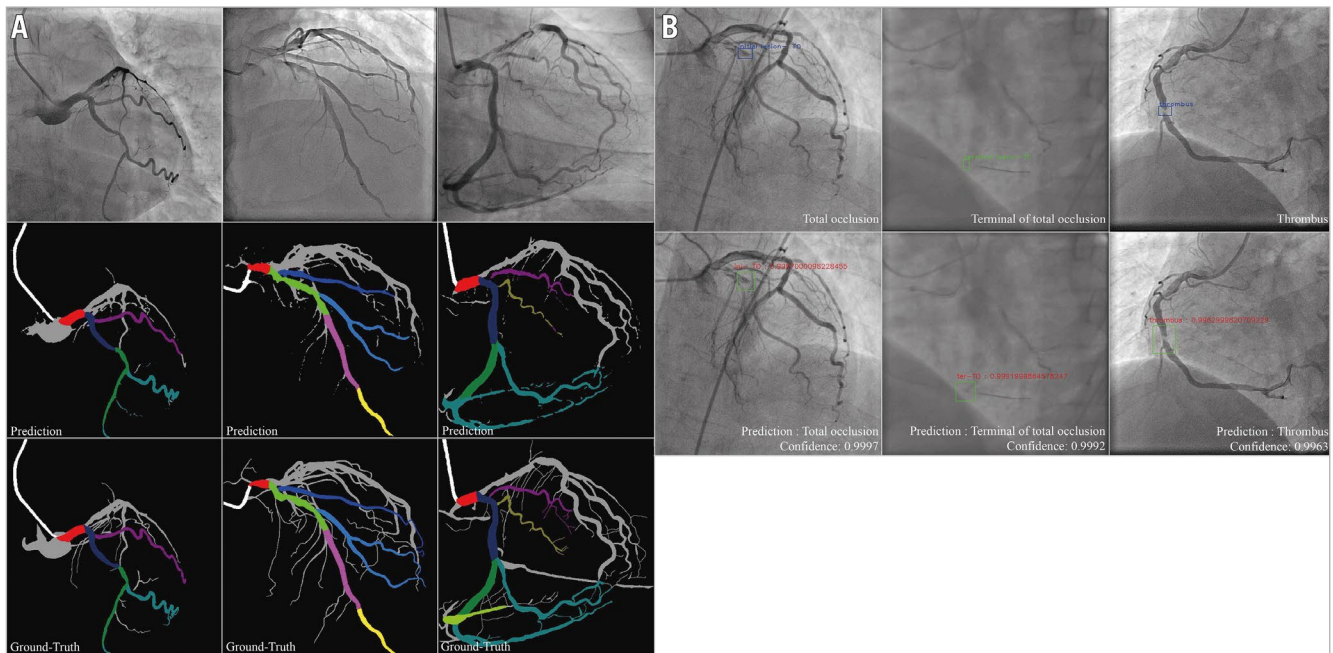


**Figure 3.** Result imaging of the segment recognition model and the lesion morphology detection model. A) Segment recognition. First row: input angiograms. Second row: resulting images generated by DeepDiscern segment recognition DNN. Third row: ground-truth labelled images. Different identified areas represent the different coronary segments. B) Lesion morphology detection. First row: input angiograms and ground-truth bounding boxes. There is a TO morphology in the first and second angiograms, and a thrombus morphology in the third angiogram in this row. Second row: bounding boxes and lesion types generated by the DeepDiscern lesion morphology detection model.

DNN for stenotic lesion, TO, calcification, thrombus, and dissection was 0.801, 0.759, 0.799, 0.778, and 0.863, respectively.

The DeepDiscern system provides an automatic and multi-modal diagnosis in a two-step process. DeepDiscern first recognises all the arterial segments in the angiogram, and then it detects the lesions in the angiogram. Processing these two steps took less

than two seconds on average for every angiogram (1.280 seconds for the segment recognition task, and 0.648 seconds for the lesion detection task). Combining these two results, DeepDiscern can analyse all lesions appearing in an angiogram (**Figure 5**).

## Discussion

Many deep learning techniques that focus on a single aspect of the coronary angiogram and coronary computed tomography analysis, and therefore do not provide a high-level analysis, have been described previously<sup>9-14</sup>. Although a single neural network has been applied to medical imaging and other medical signals to generate high-level diagnosis<sup>16-18</sup>, these approaches are different from the DeepDiscern system, which provides a coronary diagnostic map by integrating multiple aspects, including the identification of different coronary artery segments, and the recognition of lesion location and lesion type. Because of the challenges of solving the complexities of coronary angiography using a single end-to-end DNN, DeepDiscern uses multiple DNN to solve multiple sub-problems and combines the results of multiple DNN to produce a high-level diagnosis.

With the current global population expansion, the number of patients with cardiovascular disease is increasing, resulting in a growing workload for cardiologists. DeepDiscern is capable of analysing a coronary angiogram in just a few seconds by learning and understanding medical knowledge from massive medical data. DeepDiscern can be used as an assistant to analyse lesion information quickly and help cardiologists to flag and diagnose lesion

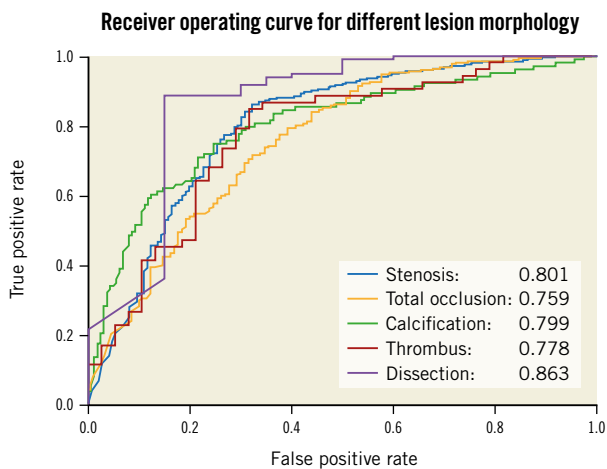


**Figure 4.** ROC curves and AUC values of all lesions. DeepDiscern lesion detection DNN predict several bounding boxes, which may contain lesion morphologies. The bounding box with a correct location and a correct type is a positive sample. The bounding box with a wrong location or a wrong type is a negative sample.

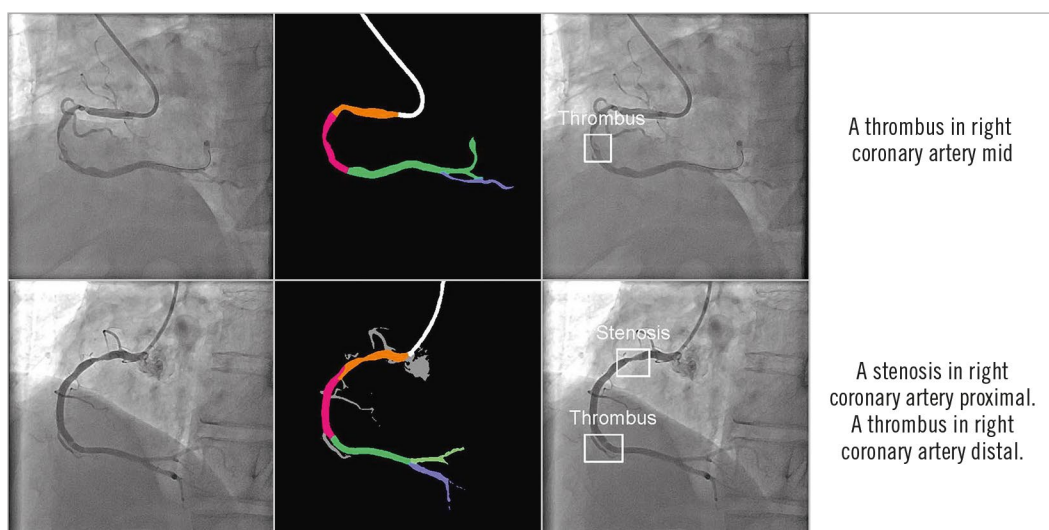


**Figure 5.** Combined results of DeepDiscern. In the first column are original angiograms. In the second column are resulting images of artery recognition DNN, where black areas represent background, white areas represent catheter, and other different colours represent different coronary artery segments. In the third column are resulting images of detection DNN. The location of lesion morphology on the angiogram is marked by several boundary boxes. The type of morphology is also predicted. In the fourth column are the combined results of recognition DNN and detection DNN.

severity and morphology during the intervention before making a treatment decision. In addition, the amount of medical documentation routinely recorded has grown exponentially and now takes up to a quarter to a half of doctors' time<sup>19</sup>. DeepDiscern can generate detailed angiographic reports automatically, saving cardiologists significant time for patient care. Thus, this approach has the potential to reduce workload and improve efficiency in coronary angiography diagnostics.

In clinical practice, visual interpretations of coronary angiograms by individuals are highly variable<sup>20</sup>. Inevitable subjective bias can have a great impact on diagnosis and treatment decisions<sup>21</sup>. Unlike the interpretation of cardiologists, the evaluation criteria of DeepDiscern are consistent for the same data set. In addition, deep learning has the ability to extract features automatically in digital angiographic images at a pixel scale, thereby impacting on angiographic interpretation by allowing analysis of angiographic images and identification of lesion features that are hard to discern by the human eye. Thus, the diagnosis of DeepDiscern is intended to be objective, accurate and reproducible.

DeepDiscern could also alleviate the growing problem of unequal distribution of medical resources and access to advanced health care. In 2017, at least half of the world's population was unable to access essential health services<sup>22</sup>. In China, the difference between the highest value of healthcare access and quality (HAQ) and the lowest is 43.5 (the highest in Beijing is 91.5 and the lowest in Tibet is 48.0)<sup>23</sup>. The number of cardiovascular disease patients in China has reached 290 million. There are more than 2,000 primary hospitals in China providing coronary intervention treatment, with levels of diagnosis and treatment differing from place to place. The DeepDiscern technology can be

extended easily and rapidly to major hospitals in the country and even the world. Implementing the DeepDiscern technology in primary hospitals countrywide could relieve the high demand for trained cardiologists, who are scarce, and provide consistency for improving angiographic diagnostic accuracy and treatment decisions, thereby achieving homogenisation of medical standards.

In the future, we will develop coronary artery lesion diagnostic systems that analyse more types of lesion morphology such as trifurcation, bifurcation, and severe tortuosity, among others. Thereafter, many decision-making tools based on recognition of lesion morphology and coronary artery segments can be automated without manual discrimination. For example, the SYNTAX score is a decision-making tool in interventional cardiology, which is determined simply by anatomical features in an angiogram<sup>24</sup>. The automation of SYNTAX score calculation is of great significance for the diagnosis of coronary angiography as it is an important tool for treatment selection (bypass surgery or percutaneous coronary intervention) in patients with more extensive CAD. The expected automatic SYNTAX score calculation system can generate a result in half a minute, detailing all the information about lesions that appear on a patient's coronary arteries (**Supplementary Figure 7**).

## Limitations

This study has several limitations. In this initial iteration, the input of DeepDiscern was a single frame angiogram obtained from an angiographic DICOM file, which provides limited information compared to a DICOM video. In actual use, after the procedure starts, the video stream of the contrast image is transmitted to our device. We used an automatic algorithm to extract a single frame with optimal contrast opacification and visualisation of the

coronary artery tree and then used this single frame image as the input for DeepDiscern. The diagnosis of coronary lesions is based on the dynamic evaluation of lesion characteristics assessed in multiple coronary angiographic views. Additionally, DeepDiscern has a large requirement for training data volume. The lack of training data can seriously affect the recognition accuracy. In general, models trained with more data have better performance. Moreover, all the angiograms used for training and testing were collected from a large single centre; therefore, external validation by using data from other centres is warranted.

## Conclusions

Deep learning technology can be used in the interpretation of diagnostic coronary angiography. In the future it may serve as a more powerful tool to standardise screening and risk stratification of patients with CAD.

### Impact on daily practice

In clinical practice, inevitable subjective bias can have a great impact on diagnosis and treatment decisions. Unlike interpretation by cardiologists, the evaluation criteria of DeepDiscern are consistent for the same data set. In addition, DeepDiscern can analyse angiographic images and identify lesion features that are hard to discern by the human eye, which can also impact on angiographic interpretation. Thus, the diagnosis of DeepDiscern is intended to be objective, accurate and reproducible.

## Funding

The study was supported by Beijing Municipal Science & Technology Commission - Pharmaceutical Collaborative Technology Innovation Research (Z18110700190000) and Chinese Academy of Medical Sciences - Medical and Health Science and Technology Innovation Project (2018-I2M-AI-007).

## Conflict of interest statement

B. Xu reports grants from Beijing Municipal Science & Technology, and grants from the Chinese Academy of Medical Sciences during the conduct of the study. In addition, B. Xu has a patent for a method of coronary artery segmentation and recognition based on deep learning pending, and a patent for an automatic detection method system, and equipment of coronary artery disease based on deep learning pending. H. Zhang reports grants from Beijing Municipal Science & Technology during the conduct of the study. The other authors have no conflicts of interest to declare.

## References

1. GBD 2013 Mortality and Causes of Death Collaborators. Global, regional, and national age-sex specific all-cause and cause-specific mortality for 240 causes of death, 1990–2013: a systematic analysis for the Global Burden of Disease Study 2013. *Lancet*. 2015;385:117-71.
2. World Health Organization. Global atlas on cardiovascular disease prevention and control. Geneva: World Health Organization; 2011. [https://www.who.int/cardiovascular\\_diseases/publications/atlas\\_cvd/en/](https://www.who.int/cardiovascular_diseases/publications/atlas_cvd/en/)

3. Dweck MR, Doris MK, Motwani M, Adamson PD, Slomka P, Dey D, Fayad ZA, Newby DE, Berman D. Imaging of coronary atherosclerosis - evolution towards new treatment strategies. *Nat Rev Cardiol*. 2016;13:533-48.
4. Authors/Task Force members, Windecker S, Kolh P, Alfonso F, Collet JP, Cremer J, Falk V, Filippatos G, Hamm C, Head SJ, Juni P, Kappetein AP, Kastrati A, Knuuti J, Landmesser U, Laufer G, Neumann FJ, Richter DJ, Schauerte P, Sousa Uva M, Stefanini GG, Taggart DP, Torracca L, Valgimigli M, Wijns W, Witkowski A. 2014 ESC/EACTS guidelines on myocardial revascularization: The Task Force on Myocardial Revascularization of the European Society of Cardiology (ESC) and the European Association for Cardio-Thoracic Surgery (EACTS) Developed with the special contribution of the European Association of Percutaneous Cardiovascular Interventions (EAPCI). *Eur Heart J*. 2014;35:2541-619.
5. Rogers MA, Aikawa E. Cardiovascular calcification: artificial intelligence and big data accelerate mechanistic discovery. *Nat Rev Cardiol*. 2019;16:261-74.
6. Beam AL, Kohane IS. Translating Artificial Intelligence into Clinical Care. *JAMA*. 2016;316:2368-9.
7. Esteva A, Kuprel B, Novoa RA, Ko J, Swetter SM, Blau HM, Thrun S. Dermatologist-level classification of skin cancer with deep neural networks. *Nature*. 2017;542:115-8.
8. Golden JA. Deep Learning Algorithms for Detection of Lymph Node Metastases from Breast Cancer: Helping Artificial Intelligence Be Seen. *JAMA*. 2017;318:2184-6.
9. Nasr-Esfahani E, Karimi N, Jafari MH, Sorousmehr SMR, Samavi S, Nallamothu BK, Najarian K. Segmentation of vessels in angiograms using convolutional neural networks. *Biomed Signal Proces*. 2018;40:240-51.
10. Jun TJ, Kweon J, Kim YH, Kim D. T-Net: Nested encoder-decoder in encoder-decoder architecture for the main vessel segmentation in coronary angiography. *Neural Netw*. 2020;128:216-33.
11. Wolterink JM, van Hamersvelt RW, Viergever MA, Leiner T, Isgum I. Coronary artery centerline extraction in cardiac CT angiography using a CNN-based orientation classifier. *Med Image Anal*. 2019;51:46-60.
12. Wolterink JM, Leiner T, Viergever MA, Isgum I. Generative Adversarial Networks for Noise Reduction in Low-Dose CT. *IEEE Trans Med Imaging*. 2017;36:2536-45.
13. Wolterink JM, Leiner T, Isgum I. Blood Vessel Geometry Synthesis using Generative Adversarial Networks. arXiv 2018; published online April 4. arXiv:1804.04381 (preprint).
14. Hwang YN, Lee JH, Kim GY, Shin ES, Kim SM. Characterization of coronary plaque regions in intravascular ultrasound images using a hybrid ensemble classifier. *Comput Methods Programs Biomed*. 2018;153:83-92.
15. Pompa J, Almonacid A, Burke D. Qualitative and Quantitative Angiography. In: Topol E, Teirstein P, editors. *Textbook of Interventional Cardiology*, 6th ed. New York, USA: Elsevier; 2011. pp 757-775.
16. Hannun AY, Rajpurkar P, Haghpanahi M, Tison GH, Bourn C, Turakhia MP, Ng AY. Cardiologist-level arrhythmia detection and classification in ambulatory electrocardiograms using a deep neural network. *Nat Med*. 2019;25:65-9.
17. Walsh SLF, Calandriello L, Silva M, Sverzellati N. Deep learning for classifying fibrotic lung disease on high-resolution computed tomography: a case-cohort study. *Lancet Respir Med*. 2018;6:837-45.
18. Gurovich Y, Hanani Y, Bar O, Nadav G, Fleischer N, Gelbman D, Basel-Salmon L, Krawitz PM, Kamphausen SB, Zenker M, Bird LM, Gripp KW. Identifying facial phenotypes of genetic disorders using deep learning. *Nat Med*. 2019;25:60-4.
19. Clynch N, Kellett J. Medical documentation: part of the solution, or part of the problem? A narrative review of the literature on the time spent on and value of medical documentation. *Int J Med Inform*. 2015;84:221-8.
20. Beauman GJ, Vogel RA. Accuracy of individual and panel visual interpretations of coronary arteriograms; implications for clinical decisions. *J Am Coll Cardiol*. 1990;16:108-13.
21. Généreux P, Palmerini T, Caixeta A, Cristea E, Mehran R, Sanchez R, Lazar D, Jankovic I, Corral MD, Dressler O, Fahy MP, Parise H, Lansky AJ, Stone GW. SYNTAX score reproducibility and variability between interventional cardiologists, core laboratory technicians, and quantitative coronary measurements. *Circ Cardiovasc Interv*. 2011;4:553-61.
22. World Health Organization. Tracking universal health coverage: 2017 Global Monitoring Report. Geneva: World Health Organization; 2017. [https://www.who.int/healthinfo/universal\\_health\\_coverage/report/2017/en/](https://www.who.int/healthinfo/universal_health_coverage/report/2017/en/)
23. GBD 2016 Healthcare Access and Quality Collaborators. Measuring performance on the Healthcare Access and Quality Index for 195 countries and territories and selected subnational locations: a systematic analysis from the Global Burden of Disease Study 2016. *Lancet*. 2018;391:2236-71.
24. Sianos G, Morel MA, Kappetein AP, Morice MC, Colombo A, Dawkins K, van den Brand M, Van Dyck N, Russell ME, Mohr FW, Serruys PW. The SYNTAX Score: an angiographic tool grading the complexity of coronary artery disease. *EuroIntervention*. 2005;1:219-27.

## Supplementary data

**Supplementary Appendix 1.** Implementation detail about coronary artery recognition network.

**Supplementary Appendix 2.** Implementation detail about lesion morphology detection network.

**Supplementary Figure 1.** The annotation procedure for coronary artery recognition and lesion morphology detection.

**Supplementary Figure 2.** Annotated coronary artery segments.

**Supplementary Figure 3.** The structure of the coronary artery recognition network.

**Supplementary Figure 4.** The structure of the lesion morphology detection network.

**Supplementary Figure 5.** Evaluation process of the coronary artery recognition model and the lesion morphology detection model.

**Supplementary Figure 6.** Performance of vessel extraction.

**Supplementary Figure 7.** Expected automatic calculation system for the SYNTAX score.

**Supplementary Table 1.** Coronary arteries labelled in different angiographic views.

**Supplementary Table 2.** National Heart, Lung and Blood Institute (NHLBI) coronary dissection criteria.

**Supplementary Table 3.** The mapping relationship between prediction label value and coronary artery segments.

**Supplementary Table 4.** Recognition performance of all segments under different angiographic views.

*The supplementary data are published online at:*

*<https://eurointervention.pronline.com/>*

*[doi/10.4244/EIJ-D-20-00570](https://doi.org/10.4244/EIJ-D-20-00570)*



## Supplementary data

### Supplementary Appendix 1. Implementation detail about coronary artery recognition network

#### *Model structure*

Existing DNN algorithms usually predict the category of each pixel. The pixel-level accuracy may be high, but the relationship between pixels is easily overlooked, making the vessel segmentation results discontinuous. Thus, we modified a special DNN: conditional generative adversarial network (cGAN) (**Supplementary Figure 4**) for image segmentation (so-called pix2pix, pix2pixHD). This cGAN consists of a generator and a discriminator. The training process of this cGAN can be treated as a competitive procedure between the generator and the discriminator. In the end, the entire model reaches Nash equilibrium. In the evaluation process, we only apply the generator to generate artery recognition results. The generator takes the coronary angiogram input and outputs the coronary artery category to which each pixel belongs. We rearrange the prediction results of each pixel into an image, indicating the recognition result of DNN. The size of the input angiogram and the output image result is 512×512 pixels.

In the generator, we apply the U-net structure with four down-sampling blocks (down-sample the input from 512×512 to 32×32) and four up-sampling blocks (up-sample the input from 32×32 to 512×512) as the generator part, which is shown in **Supplementary Figure 4**. The discriminator part contains three sub-discriminators to discriminate on three different scales and average the results. The three distinguishing scales are the original image, 1/2 down-sampling of the original image, and 1/4 down-sampling of the original image. These three layers build an image pyramid and train a discriminator for each layer. It is notable that we use a convolutional “PatchGAN” classifier in these sub-discriminators, which only penalises structure at the scale of image patches. More specifically, each sub-discriminator outputs an 8×8 matrix. Each element of this matrix is a single value (from 0 to 1) corresponding to a 64×64 patch of input. Each sub-discriminator tries to classify if each 64×64 patch in an image is real or fake. We run this discriminator convolutionally across the image, averaging all responses to provide the ultimate output of sub-discriminator. This design can significantly improve the spatial continuity of segmentation results.

In the network testing process, the outputs of the generator are treated as segmentation results. The output has three RGB channels (a GAN model output has the same shape as its input). Each pixel in the output will be converted to a prediction label according to the Euclidean distance between pixel value and prediction label value. The mapping relationship between prediction label value and coronary artery segments is shown in **Supplementary Table 4**. For example, a predicted pixel (250,249,248) will be converted to the label value (255,255,255), which has the minimal Euclidean distance to this predicted pixel. Different kinds of ground-truth triad value only contain 0,128 or 255, which ensures the large Euclidean distance between different ground-truth values so that each pixel will eventually converge to its ground-truth label. However, the model will publish various kinds of misclassified pixels differently in the initial stage of network training, which slows down the network training.

Multiple-channel output (21 one-hot channels) may improve the issue even though it increases the amount calculation slightly. In this work, we set the output as 3 RGB image.

### **Loss function**

(1) GAN loss.

The optimisation process of our Conditional GANs can be described as the following minimax game:

$$\min_G \max_D L_{GAN}(G, D),$$

Where the loss function  $L_{GAN}(G, D)$  is given by

$$E_{(i,o)}[\log D(i, o)] + E_{(i)}[\log (1 - D(i, G(i)))],$$

where  $i$  is an angiogram and  $o$  is a segmentation result image. Our discriminator part has three sub-discriminators. The learning problem then becomes a multi-task learning problem of

$$\min_G \max_{D_1 D_2 D_3} \sum_{k=1,2,3} L_{GAN}(G, D_k).$$

(2) Feature matching loss.

In each sub-discriminator, we calculated the pixel-wise loss between the feature of the generated segmentation result by generator and the feature of the ground truth. The loss is shown as:

$$L_{FM}(G, D_k) = \sum_{i=1}^T \frac{1}{N_i} \|D_k^{(i)}(i, o) - D_k^{(i)}(i, G(i))\|_1,$$

where  $T$  is the total number of layers (herein there are five layers in each sub-discriminator),  $N_i$  denotes the number of elements in each layer,  $D_k^{(i)}$  denotes the  $i$ th-layer feature extractor of sub-discriminator  $D_k$ .

(3) VGG-based perceptual loss.

Like feature matching loss, we also extract the VGG feature of the generated segmentation result by generator and the VGG feature of the ground truth, considering the low-level feature (edge and context) extracted by pre-trained VGG network, also avails angiogram analysis. The loss is shown as:

$$L_{VGG}(G, D_k) = \sum_{j=1}^N \frac{1}{M_j} \|VGG^{(j)}(o) - VGG^{(j)}(G(i))\|_1,$$

where  $N$  is the total number of VGG layers,  $M_j$  denotes the number of elements in each layer,  $VGG_k^{(j)}$  denotes the  $j$ th-layer feature extractor of VGG.

The total loss function is the sum of the above three losses, shown as:

$$\min_G \max_{D_1 D_2 D_3} \sum_{k=1,2,3} L_{GAN}(G, D_k) + \alpha \sum_{k=1,2,3} L_{FM}(G, D_k) + \beta \sum_{k=1,2,3} L_{VGG}(G, D_k)$$

### **Implementation detail**

For training, the initial learning rate is  $2 \times 10^5$ , which gradually dropped to  $10^6$  during training. For the weight parameter, we set  $\alpha$  as 0.5 and  $\beta$  as 10. The number of training epochs is 400.

Graphics processing units are NVIDIA GTX 1080Ti GPUs. Adam optimiser was used to optimise our model. Training time lasted about five days.

## Supplementary Appendix 2. Implementation detail about lesion morphology detection network

### Model structure

For the lesion morphology detection task, we developed a convolutional DNN (**Supplementary Figure 4**), which takes coronary angiogram input and outputs the location (the upper left and lower right coordinates of the predicted rectangular area) and type (a scalar) of all the lesion morphologies that appeared in the input angiogram. Deep residual block, up-sampling layer, and lateral connection are used to extract different scale features of different lesions. Using these feature maps, the Region Proposal Network generates region proposal areas where lesion morphologies may occur. After that, features of every region proposal area are fed into convolutional layers and fully connected layers, to predict the type and location of lesion morphologies.

As shown in **Supplementary Figure 5**, the input angiograms are down-sampled by  $2 \times 2$  pooling layers and up-sampled by  $2 \times 2$  interpolated layers. Different down-sampling features and up-sampling features are combined by element-sum (light green arrows) operator. Convolutional layers (green arrows) extract four different scale detection features. Using these feature maps, RPN (region proposal network) generates region proposal areas where lesion morphologies may occur. After that, features of every region proposal area are fed into several convolutional layers and fully connected layers, to predict the type and location of lesion morphologies.

We treated four different scale detection features (dark blue blocks as  $F_0, F_1, F_2, F_3$ ) as a feature pyramid and viewed it as if it were produced from an image pyramid. Thus, we can adapt the assignment strategy of region-based detectors (in Fast r-cnn) in the case when they run on image pyramids. Formally, we assign a region of interest (RoI) of width  $w$  and height  $h$  (on the input image to the network) to the level  $F_k$  of our feature pyramid by:  $k = \lfloor k_0 + \log_2(\sqrt{wh}/224) \rfloor$ . Here  $k_0$  is the target level on which an RoI with  $w \times h = 224^2$  should be mapped into. We set  $k_0$  to 3. Intuitively, the equation above means that if the RoI's scale becomes smaller (say,  $1/2$  of 224), it should be mapped into a finer-resolution level (say,  $k = 2$ ).

### Loss function

After assigning the detection feature for a RoI, the optimisation process of our lesion detection network can be described as:

$$L(p_i, t_i) = \frac{1}{N_{cls}} \sum_i L_{cls}(p_i, p_i^*) + \lambda \frac{1}{N_{reg}} \sum_i p_i^* L_{reg}(t_i, t_i^*)$$

Where  $p_i$  is the classification possibility of the  $i$ th anchor (the region proposal box generated by RPN, presented by a four tuple  $\{x_1, y_1, x_2, y_2\}$ , where  $(x_1, y_1)$  is the left-top corner of the box and  $(x_2, y_2)$  is the right-bottom corner of the box), we name the  $i$ th anchor as Anchor[ $i$ ].

When the Anchor[ $i$ ] is positive region proposal (the IOU of Anchor[ $i$ ] and its Ground Truth Box  $> 0.7$ ),  $p_i^* = 1$ . When the Anchor[ $i$ ] is negative region proposal (the IOU of Anchor[ $i$ ] and its Ground Truth Box  $< 0.3$ ),  $p_i^* = 0$ . Anchors that are not positive or negative were not trained by the network.  $t_i$  is the

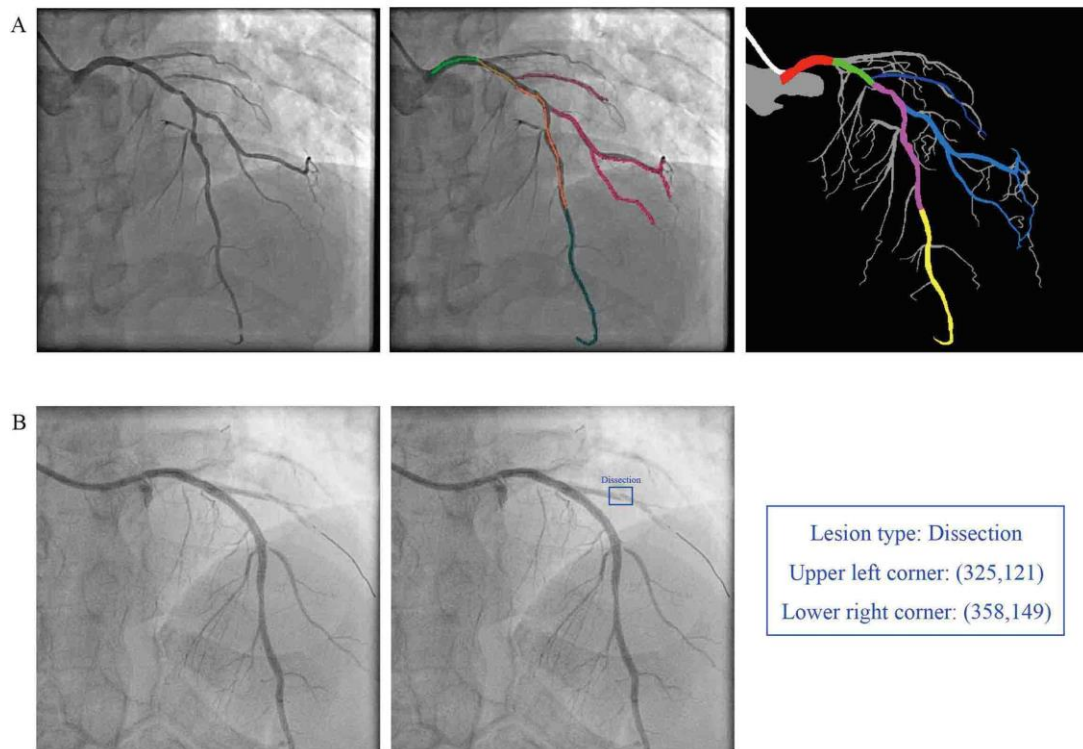
parameterised coordinates of the predicted box of Anchor[i], and  $t_i^*$  is the parameterised coordinates of the Ground Truth Box of Anchor[i].

For an anchor box,  $t_i = \{t_x, t_y, t_w, t_h\}$  where  $t_x = (x - x_a/w_a)$ ,  $t_y = (y - y_a/h_a)$ ,  $t_w = \log(w/w_a)$ ,  $t_h = \log(h/h_a)$ ;  $t_i^* = \{t_x^*, t_y^*, t_w^*, t_h^*\}$  where  $t_x^* = (x^* - x_a/w_a)$ ,  $t_y^* = (y^* - y_a/h_a)$ ,  $t_w^* = \log(w^*/w_a)$ ,  $t_h^* = \log(h^*/h_a)$ , where  $(x, y)$  is the centre point of the predicted box,  $w, h$  are the weight and height of the predicted box,  $(x_a, y_a)$  is the centre point of the anchor box,  $w_a, h_a$  are the weight and height of the anchor box,  $(x^*, y^*)$  is the centre point of the Ground Truth box,  $w^*, h^*$  are the weight and height of the Ground Truth box.

$N_{cls}$  is the minibatch size.  $N_{reg}$  is the number of anchor box.  $L_{cls}(p_i, p_i^*) = -\log [p_i p_i^* + (1 - p_i)(1 - p_i^*)]$  and  $L_{reg}(t_i, t_i^*) = Smooth_{L1}(t_i - t_i^*)$  where  $Smooth_{L1}(x) = \begin{cases} 0.5 * x^2 & |x| < 1 \\ |x| - 0.5 & otherwise \end{cases}$ .

### ***Implementation details***

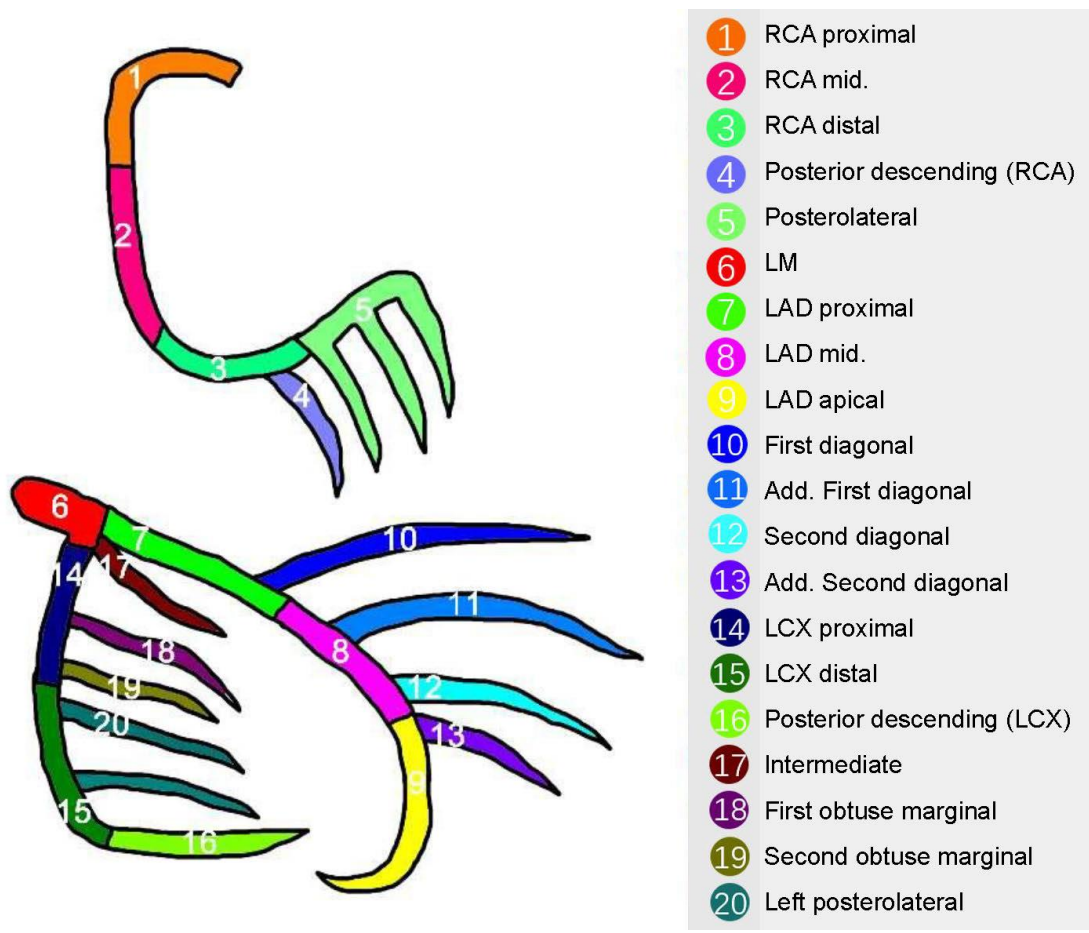
All architectures in **Supplementary Figure 4** are trained end to end. We adopt synchronised SGD optimiser to update our network. Graphics processing units are NVIDIA GTX 1080Ti GPUs. A mini-batch involves two images and 256 anchors per image. We use a weight decay of 0.0001, a momentum of 0.9 and a  $\lambda$  of 10. The learning rate is 0.02 for the first 30k mini-batches and 0.002 for the next 10k. The implementation details of FPN feature selection are set the same as in FPN (feature pyramid networks).



**Supplementary Figure 1.** The annotation procedure for coronary artery recognition and lesion morphology detection.

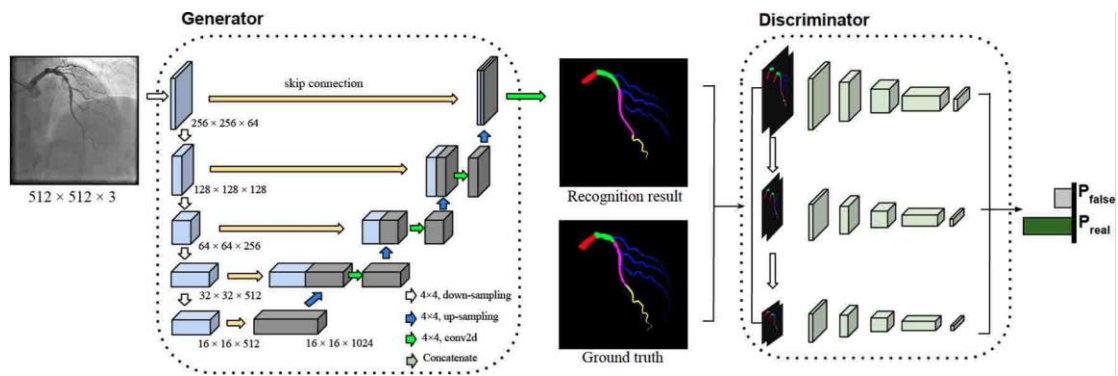
A) Coronary artery recognition. The first image is an original image. The second image is a sketchy-labelled image. The third image is a fine-labelled image.

B) Lesion morphology detection. The first image is an original image. The second image is a labelled image including lesion type and lesion location.



**Supplementary Figure 2.** Annotated coronary artery segments.

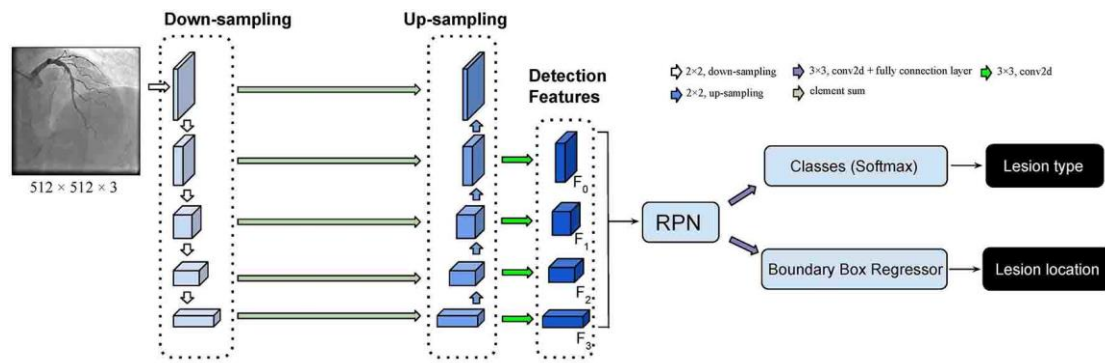
A total of 20 coronary artery segments were annotated in our study.



**Supplementary Figure 3.** The structure of the coronary artery recognition network.

This GAN consists of a generator and a discriminator. The training process of this network can be treated as a competitive procedure between the generator and the discriminator. In the end, the entire model reaches Nash equilibrium and the accuracy of the discriminator is equal to 50%, which means that the discriminator is hard to discern the difference between recognition results and ground-truth images, showing that generator outputs a high-quality recognition result. In the evaluation process, we only apply the generator to generate artery recognition results.

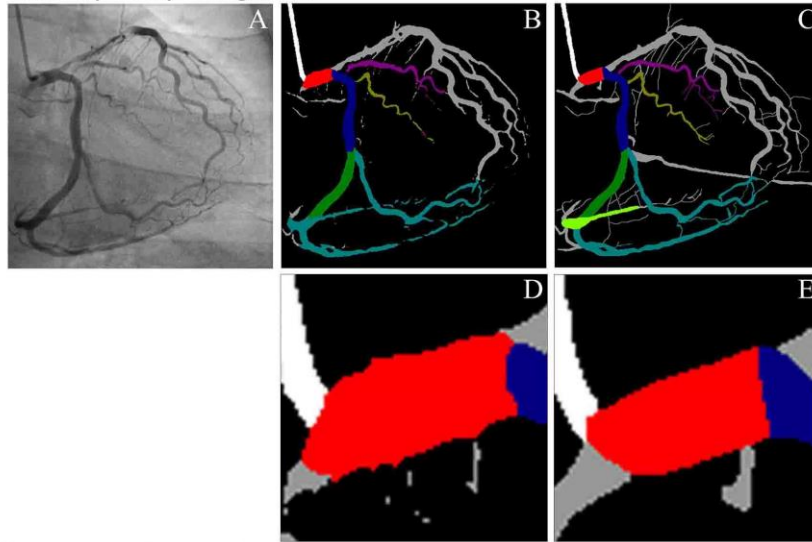
In the generator, the input angiograms are down-sampled (white arrows) and then up-sampled (blue arrows) to generate features of different scale. These features are combined by concatenated operator (yellow arrows) to enrich the semantic information for better performance. In the discriminator, recognition results and ground truth are resized to different scale and processed and combined by several convolutional layers to generate the discrimination result.



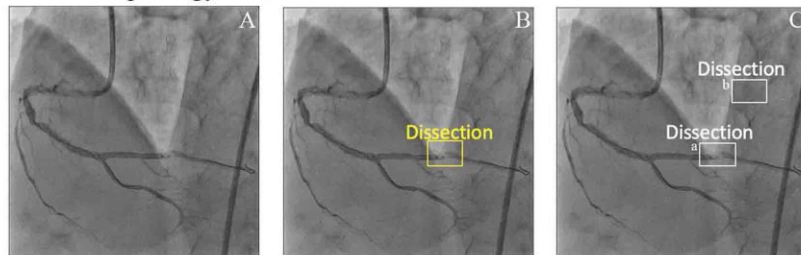
**Supplementary Figure 4.** The structure of the lesion morphology detection network.

The input angiograms are down-sampled by  $2 \times 2$  pooling layers and up-sampled by  $2 \times 2$  interpolated layers. Different down-sampling features and up-sampling features are combined by element-sum (light green arrows) operator. Convolutional layers (green arrows) extract four different scale detection features. Using these feature maps, the RPN network generates region proposal areas where lesion morphologies may occur. After that, features of every region proposal area are fed into several convolutional layers and fully connected layers, to predict the type and location of lesion morphologies. RPN: region proposal network

### Coronary artery recognition



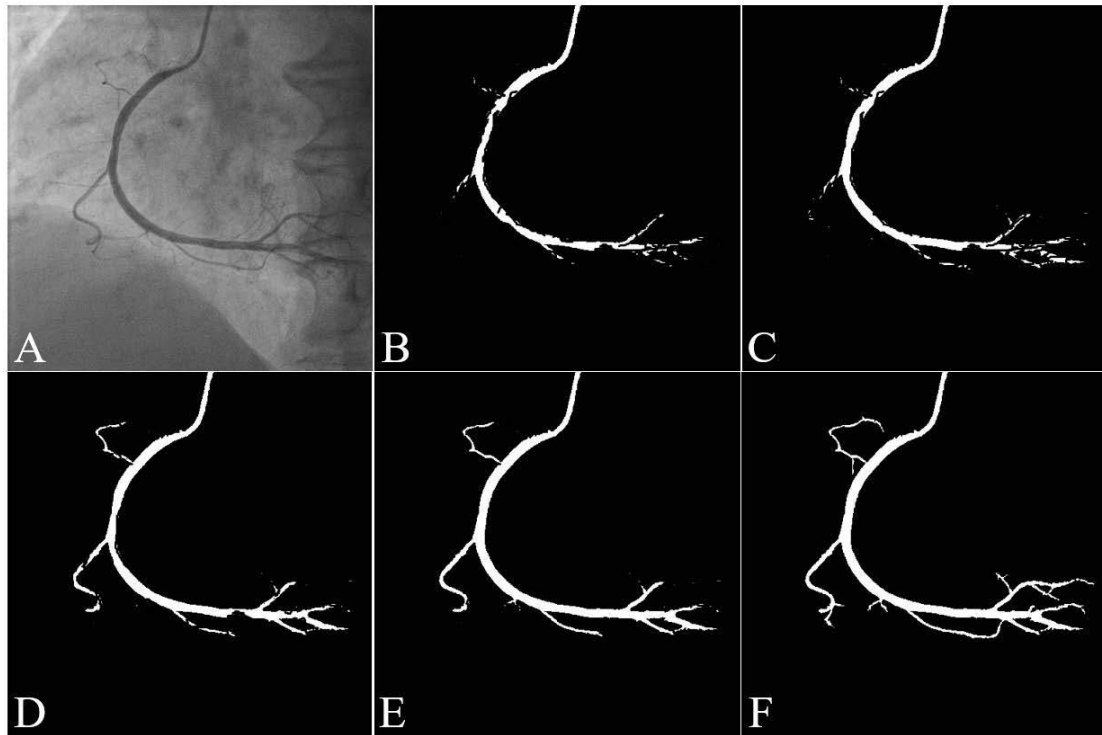
### Lesion morphology detection



**Supplementary Figure 5.** Evaluation process of the coronary artery recognition model and the lesion morphology detection model.

For the coronary artery recognition model, we feed an angiogram (A) as input image. The recognition model will output the results (C). The middle image is ground truth (B). D and E are generated by zooming in the LM segment in B and C. In the result image, the red area is the predicted area of the LM segment by the model. We counted the number of red pixels in this area (E) and ground-truth area (D) to calculate the pixel number of true positive (TP), true negative (TN), false positive (FP) and false negative (FN). The TP pixel is the red pixel in D and E. The TN pixel is the non-red pixel in D and E. The FP pixel is the red pixel in E but the non-red pixel in D. The FN pixel is the non-red pixel in E but the red pixel in D. Based on these results, we evaluate the segment recognition model by several metrics including accuracy ( $(TP+TN)/(TP+TN+FP+FN)$ ), sensitivity ( $TP/(TP+FN)$ ), specificity ( $TN/(TN+FP)$ ), positive predictive value ( $TP/(TP+FP)$ ), negative predictive value ( $TN/(TN+FN)$ ). For the lesion morphology detection model, we feed an angiogram (A) as input. The detection model will output the results (C). The yellow bounding box and lesion name are ground truth (B). The white bounding boxes are detected lesion cases by models. One dissection lesion (a, overlap rate=0.90 >0.5) is detected correctly, and another one (b, overlap rate=0 <0.5) is detected incorrectly. For this angiogram, the precision rate is 50%, the recall rate is 100% and the F1 score is 0.667. We counted all detected lesion cases by models and all correctly

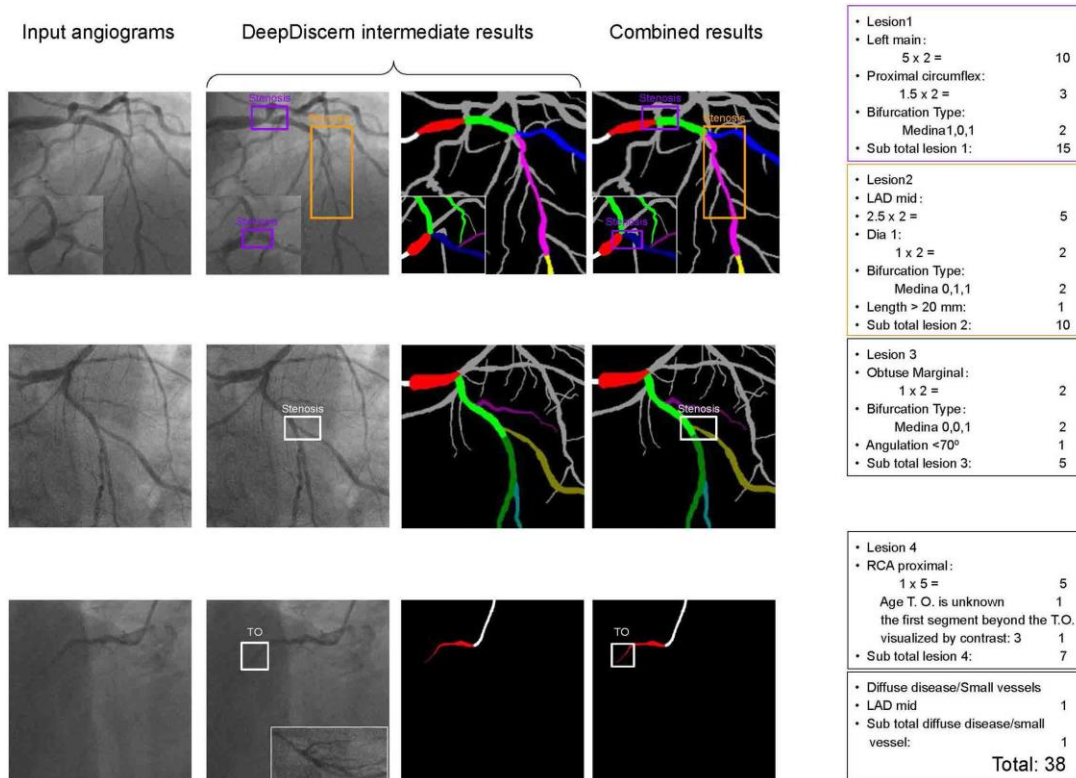
detected lesion cases in the test data set to calculate the precision rate, recall rate and F1 score of every kind of lesion.



**Supplementary Figure 6.** Performance of vessel extraction.

A) Input angiogram.

B) – F) Result images of recognition models which were trained using a different amount of data (1,000, 3,000, 5,500, 8,000, 11,900 images).



**Supplementary Figure 7.** Expected automatic calculation system for the SYNTAX score.

First column: input angiograms under different angiographic views. Second and third columns: the intermediate results generated by DeepDiscern system. Fourth column: combined results. All images are zoomed in for better visualisation.

**Supplementary Table 1. Coronary arteries labelled in different angiographic views.**

Coronary artery segments	CRA <sup>b</sup>	CAU <sup>b</sup>	LAO (right) <sup>a</sup>		RAO_CAU <sup>b</sup>	RAO_CRA <sup>b</sup>
			LAO_CAU (right) <sup>a</sup>	LAO_CRA (right) <sup>a</sup>		
			LAO_CAU (right) <sup>a</sup>	LAO_CRA (right) <sup>a</sup>		
LM	√	√	√	√	√	√
LAD proximal	√		√	√		√
First diagonal	√		√	√		√
Add. first diagonal	√		√	√		√
LAD mid	√		√	√		√
Second diagonal	√			√		√
Add. second diagonal	√			√		√
LAD apical	√		√	√		√
Intermediate		√		√	√	
LCX proximal		√		√	√	
LCX distal		√		√	√	
Second obtuse marginal		√		√	√	
First obtuse marginal		√		√	√	
Left posterolateral		√		√	√	
Posterior descending (LCX)		√		√	√	
RCA proximal			√			
RCA mid.			√			
RCA distal			√			
Posterior descending (RCA)			√			
Posterolateral			√			
Unconcerned arteries <sup>c</sup>	√	√	√	√	√	√
Background	√	√	√	√	√	√
Catheter	√	√	√	√	√	√

DIA: diagonal; LAD: left anterior descending artery; LCX: left circumflex artery; LM: left main; L-PDA: left posterior descending; L-PLA: left posterolateral; OM: obtuse marginal; PDA: posterior descending; PLA: posterolateral; RCA: right coronary artery

<sup>a</sup>In the LAO\_CAU (right) part of the data set, all angiograms were obtained in the LAO\_CAU view. Only the right coronary artery appeared in these angiograms, as well as for LAO and LAO\_CRA (right) parts.

<sup>b</sup>In the other parts of the data set, all angiograms were obtained in the angiographic view corresponding to their part name. Only the left coronary artery appeared in these angiograms.

<sup>c</sup>For every part of the data set, all coronary artery segments without check marks were labelled as “unconcerned arteries”. These coronary artery segments will not be overly concerned in the angiographic view of this part of the data set.

**Supplementary Table 2. National Heart, Lung and Blood Institute (NHLBI) coronary dissection criteria.**

<b>Variable</b>	<b>Definition</b>
Dissection	
A	Small radiolucent area within the lumen of the vessel
B	Linear non-persisting extravasation of contrast
C	Extraluminal, persisting extravasation of contrast
D	Spiral – shaped filling defect
E	Persistent luminal defect with delayed anterograde flow
F	Filling defect accompanied by total coronary occlusion

**Supplementary Table 3. The mapping relationship between prediction label value and coronary artery segments.**

Coronary artery segments	Label value	Colour	Coronary artery segments	Label value	Colour
LM	(255,0,0)	■	Second obtuse marginal	(128,128,0)	■
LAD proximal	(0,255,0)	■	First obtuse marginal	(128,0,128)	■
First diagonal	(0,0,255)	■	Left posterolateral	(0,128,128)	■
Add. first diagonal	(0,128,255)	■	Posterior descending (LCX)	(128,255,0)	■
LAD mid	(255,0,255)	■	RCA proximal	(255,128,0)	■
Second diagonal	(0,255,255)	■	RCA mid	(255,0,128)	■
Add. second diagonal	(128,0,255)	■	RCA distal	(0,255,128)	■
LAD apical	(255,255,0)	■	Posterior descending (RCA)	(128,128,255)	■
Intermediate	(128,0,0)	■	Posterolateral	(128,255,128)	■
LCX proximal	(0,0,128)	■	Background	(0,0,0)	■
LCX distal	(0,128,0)	■	Catheter	(255,255,255)	■

DIA: diagonal; LAD: left anterior descending artery; LCX: left circumflex artery; LM: left main; L-PDA: left posterior descending; L-PLA: left posterolateral; OM: obtuse marginal; PDA: posterior descending; PLA: posterolateral; RCA: right coronary artery

**Supplementary Table 4. Recognition performance of all segments under different angiographic views.**

<b>Angiographic view</b>	<b>Accuracy % (95% CI)</b>	<b>Sensitivity % (95% CI)</b>	<b>Specificity % (95% CI)</b>	<b>PPV % (95% CI)</b>	<b>NPV % (95% CI)</b>
Left coronary artery					
CRA	98.5 (98.4-98.6)	86.8 (85.8-87.8)	98.9 (98.9-99.0)	74.0 (72.8-75.2)	99.5 (99.5-99.6)
CAU	98.5 (98.5-98.6)	83.8 (82.8-84.8)	98.9 (98.8-99.0)	70.8 (69.7-72.0)	99.5 (99.5-99.6)
LAO_CRA	98.4 (98.3-98.5)	86.6 (85.5-87.6)	98.8 (98.7-98.9)	70.8 (69.7-71.9)	99.5 (99.4-99.5)
LAO_CAU	98.7 (98.6-98.8)	87.8 (86.8-88.9)	99.0 (99.0-99.1)	73.4 (72.1-74.6)	99.6 (99.6-99.7)
RAO_CRA	98.4 (98.3-98.5)	86.6 (85.6-87.5)	98.8 (98.7-98.9)	71.0 (69.9-72.1)	99.5 (99.5-99.5)
RAO_CAU	99.0 (98.9-99.1)	87.8 (86.9-88.8)	99.4 (99.3-99.4)	80.3 (79.2-81.3)	99.6 (99.6-99.7)
Right coronary artery					
LAO	98.1 (98.0-98.2)	78.5 (77.2-79.7)	98.8 (98.7-98.9)	72.8 (71.5-74.2)	99.2 (99.1-99.2)
LAO_CAU	98.6 (98.5-98.6)	83.2 (82.3-84.1)	99.2 (99.1-99.2)	79.7 (78.8-80.6)	99.3 (99.2-99.4)
LAO_CRA	98.1 (97.9-98.2)	86.5 (85.8-87.3)	99.4 (99.3-99.4)	85.1 (84.3-85.9)	99.5 (99.4-99.5)
RAO	97.1 (96.8-97.3)	83.4 (81.7-85.0)	99.2 (99.1-99.3)	79.0 (77.2-80.9)	99.4 (99.3-99.5)

CAU: caudal view; CRA: cranial view; LAO: left anterior oblique view; LAO\_CAU: left anterior oblique-caudal view; LAO\_CRA: left anterior oblique-cranial view; NPV: negative predictive value; PPV: positive predictive value; RAO: right anterior oblique view; RAO\_CAU: right anterior oblique-caudal view; RAO\_CRA: right anterior oblique-cranial view